Separation of Isotopes in Space and Time by Gas-Surface Atomic Diffraction

Kevin J. Nihill, Jacob D. Graham, and S. J. Sibener

Phys. Rev. Lett. **119**, 176001 — Published 23 October 2017

DOI: 10.1103/PhysRevLett.119.176001

Separation of Isotopes in Space and Time by Gas-Surface Atomic Diffraction

Kevin J. Nihill,[1,a] Jacob D. Graham,[1,a] and S.J. Sibener[1,*]

[1] The James Franck Institute and Department of Chemistry, The University of Chicago,

929 E. 57th Street, Chicago, Illinois 60637, USA

Revised Submission to *Physical Review Letters*

a) K.J. Nihill and J.D. Graham contributed equally to this work

*Corresponding Author. Electronic mail: s-sibener@uchicago.edu

Abstract

The separation of isotopes in space and time by gas-surface atomic diffraction is presented as a new means for isotopic enrichment. A supersonic beam of natural abundance neon is scattered from a periodic surface of methyl-terminated silicon, with the ^{20}Ne and ^{22}Ne isotopes scattering into unique diffraction channels. Under the experimental conditions presented in this letter, a single pass yields an enrichment factor 3.50 ± 0.30 for the less abundant isotope, ^{22}Ne, with extension to multiple passes easily envisioned. The velocity distribution of the incident beam is demonstrated to be the determining factor in the degree of separation between the isotopes' diffraction peaks. In cases where there is incomplete angular separation, the difference in arrival times of the two isotopes at a given scattered angle can be exploited to achieve complete temporal separation of the isotopes. This study explores the novel application of supersonic molecular beam studies as a viable candidate for separation of isotopes without the need for ionization or laser excitation.

Proposals for separating and enriching isotopes came about almost immediately after isotopes were discovered. In 1919, Lindemann and Aston examined a vast array of possible methods including fractional distillation, chemical separation, gaseous diffusion, gravitational and centrifugal separation, along with separation of positive ions with electric and magnetic fields [1]. Their early analysis concluded that isotopes "must be separable in principle though possibly not in practice." The Manhattan Project in the 1940s ushered in large scale practical implementation of many of these techniques. Fractional distillation, gaseous diffusion and magnetic sector mass spectrometers (Calutrons) were all used on an industrial scale to enrich ^{235}U [2,3]. Today, isotope separation and enrichment underpins advanced technologies in a wide variety of fields, including isotopic labeling in the life science, the use of radioisotopes in medicine, and a variety of energy systems. Microelectronics may also begin to utilize isotopic enrichment as highly enriched ^{28}Si wafers have markedly increased thermal conductivity [4] and electron transport characteristics [5] over natural abundance silicon wafers. Gaseous diffusion, distillation and gas centrifuges exhibit small isotopic separation effects that are overcome through large-scale installations where many separation steps are performed in sequence. Alternatively, a variety of laser-based techniques exist [6] that are capable of separating isotopes to a much higher degree, but require ionization or excitation of the target isotope; illustrative examples include atomic vapor laser isotope separation (AVLIS) [7] and techniques such as magnetically activated and guided isotope separation (MAGIS) [8].

A rather unexplored isotope separation technique is supersonic beam diffraction. Among isotope separation methods, supersonic beam diffraction has the unique combination of being a non-ionizing/dissociative process that can achieve high separation effects. This high degree of separation is only achievable *via* the narrow velocity distribution of a supersonic beam, which

translates into a narrow angular distribution that is scattered from a highly periodic surface. While effusive beam sources have been used for atomic and molecular diffraction since pioneering experiments in the 1930s, a very small percentage of the beam flux is within a few percent of the mean beam velocity [9], preventing any meaningful degree of isotopic purification by atomic diffraction. In contrast, the advent of supersonic nozzle sources with high Mach numbers affords considerably narrower velocity distributions – here, as low as $\Delta v/v$ = 6.4%. Such narrow velocity distributions, when coupled with a high-quality, high Debye temperature surface, make separation of atomic isotopes *via* atomic diffraction feasible.

Previous work by Boato *et al.* suggested the existence of isotopically unique diffraction channels for neon scattering from LiF(001), but was unable to resolve this feature [10]. Here, the separation of the ^{20}Ne and ^{22}Ne isotopes *via* atomic diffraction is observed for the first time when a neon beam with a natural abundance of each isotope is scattered from a methyl-terminated Si(111) surface as shown schematically in Figure 1a. When paired with the extreme resolution and sensitivity of the isotopically specific scattered angle with respect to the mass differences of the incident atoms, diffraction experiments offer a promising isotope separation technique.

The ultra-high vacuum (UHV) scattering apparatus required for this experiment is illustrated in Figure 1b, and has been described in greater detail elsewhere [11]. Briefly, it is comprised of three primary sections: a differentially pumped beam source, a UHV chamber that houses the crystal, and a rotatable mass spectrometer detector. A natural abundance (90.48% ^{20}Ne and 9.25% ^{22}Ne) neon beam with a narrow energy distribution is generated by supersonically expanding ultra-high purity Ne gas through a 15 μm diameter nozzle source which is cooled by a closed-cycle helium refrigerator. The incident energy distribution of this

beam is measured with an in-line mass spectrometer and is minimized to $\Delta v/v = 6.4\%$ by adjusting the backing pressure of Ne. Similarly, the beam energy, which is determined by the nozzle temperature, is optimized to 50 K (E_B ~10 meV) in order to minimize the incident energy while avoiding the formation of clusters. For diffraction and time-of-flight measurements, a pre-collision chopper is used to modulate the beam with a duty cycle of 50%; the time-of-flight measurements are performed by modulating the beam with a pseudorandom chopping sequence for cross-correlation analysis [12]. The spatial profile of the beam is minimized by collimation through a series of apertures, resulting in a 4 mm spot size on the crystal (chopper-to-crystal distance = 0.4996 m). From this spot size, pressure rise in the scattering chamber, and the pumping speed, an incident flux of ~10^{14} $cm^{-2}s^{-1}$ was determined. After the collision with the surface, which is mounted on a six-axis manipulator in order to control the incidence angle (θ_i), azimuth (φ), and tilt (χ) of the crystal, the neon atoms travel along a 0.5782 m (crystal-to-ionizer distance) triply differentially pumped rotatable detector arm with an angular resolution of 0.29° FWHM, are ionized by electron bombardment, which is sensitive to number density, and then pass through a quadrupole mass spectrometer (QMS) before striking an electron multiplier. The QMS is adjusted to selectively filter either the ^{20}Ne or ^{22}Ne isotope. The angular distributions for diffraction scans are obtained by scanning the detector at 0.1° increments over a range of 35°, all while holding the incident angle at a fixed value. Between scattering experiments, the temperature of the crystal was flashed to 200 K to eliminate unwanted surface adsorbates and maximize elastic scattered intensity.

The crystal used for this experiment, CH_3-Si(111), was created by the Lewis group at the California Institute of Technology [13], and shipped under argon to the University of Chicago for the neon scattering experiments. This crystal was chosen for its small surface atom spacing

(3.82 Å), high surface Debye temperature (983 K) which limits diffusive scattering, and high quality and long-range periodicity achieved in the synthesis of the crystal, which is described in greater detail elsewhere [14–16].

When molecules elastically scatter from a surface, they can undergo a discrete exchange of parallel momentum ΔK with the surface, as governed by the equation

$$\Delta K = k_i \left(\sin\theta_f - \sin\theta_i \right), \tag{1}$$

where k_i is the incident wavevector of the beam, and θ_i and θ_f are, respectively, the incident and final scattered angles of the molecular beam as measured from the surface normal. This condition for elastic diffraction is met when the change in parallel momentum is equal to a sum of the reciprocal lattice vectors b_i according to the equation

$$\Delta K = h\vec{b_1} + k\vec{b_2}. \tag{2}$$

As is evident from equation (1), the angular location of a diffraction peak is determined in part by its incident wavevector (k_i), which in turn is dependent on the velocity of the incident beam.

For an elastic gas-surface interaction, the incident velocity distribution of the molecular beam can be transformed into a theoretical angular distribution of the scattered beam through the implementation of equation (1). Figure 2 shows the predicted angular distribution of Ne scattered from CH_3-Si(111) for both a supersonic molecular beam ($\Delta v/v = 6.4\%$) and an effusive beam using a Maxwell-Boltzmann distribution at a temperature of 55 K. The separation of the isotopes is nearly complete with the supersonic nozzle source, whereas the effusive source is incapable of any significant degree of isotope purification using this method.

Experimental angular scans of the (11) diffraction peak for ^{20}Ne and ^{22}Ne are shown in Figure 3. These diffraction spectra were recorded using a naturally abundant supersonic neon beam with both isotopes having the same average velocity and velocity distribution. These spectra illustrate the high degree of angular separation between the respective isotope (11) diffraction peaks and thus the feasibility of separating isotopes *via* supersonic beam diffraction. The natural abundance of the neon beam (90.48% ^{20}Ne and 9.25% ^{22}Ne) accounts for the nearly order of magnitude intensity difference for the maximum of each isotope's (11) diffraction peak. For this particular experimental condition, one can assess the efficacy of this isotopic enrichment method. As the angular resolution of the instrument is 0.67°, each point on the spectra can represent a collector with this acceptance angle. For the case of enriching the major ^{20}Ne component, the collector can be placed at the maximum of the ^{20}Ne (11) diffraction peak (θ_f = 47.5°) shown in Figure 3, which sits on top of a small incoherent background and the tail of the ^{22}Ne diffraction peak. The collected signal after scattering provides a ^{20}Ne abundance of 97.3% ± 3.0%, as compared to the original abundance of ^{20}Ne (90.48%), thus yielding an enrichment factor of 1.08 ± 0.03 (this represents 1σ error). Similarly, for the minor ^{22}Ne component, the collector can be placed at the maximum of the ^{22}Ne (11) diffraction peak (θ_f = 45.1°) shown in Figure 3, which sits on top of a small incoherent background and the tail of the ^{20}Ne diffraction peak. The collected signal after scattering provides a ^{22}Ne abundance of 32.4% ± 2.8%, as compared to the original abundance of ^{22}Ne (9.25%), thus yielding an enrichment factor of 3.50 ± 0.30. Note that these enrichment factors can be improved further by lowering the temperature of the substrate to near but above the adsorption limit, ~7 K for neon, which minimizes incoherent scattering from Debye-Waller effects for given incident kinematics.

The large but still incomplete spatial separation of the isotopes' diffraction peaks is primarily due to the width of these features. To emphasize this point, Figure 4 shows helium and neon scattering from CH_3-Si(111), with the width of the diffraction peaks for these species resulting from the convolution of the instrument function, surface quality, and their incident velocity distributions. The narrower angular distribution for He results from its considerably narrower incident velocity distribution ($\Delta v/v = 0.8\%$) as compared to that of Ne ($\Delta v/v = 6.4\%$), indicating that improvement of the beam quality will result in even greater angular separation than the data shown in Figure 3. While a common method for narrowing the velocity distribution is seeding the beam with a light gas (e.g. He, H_2) [15,17,18], the increased average velocity of this mixture would bring the angular positions of the diffraction peaks closer together, limiting the degree of separation, as predicted by equation (1). We note that this can be compensated for by cooling the nozzle of the seeded beam to regain the increased reciprocal-space distance between diffraction peaks while maintaining a narrow incident velocity distribution. An additional solution would be the addition of an in-line pre-collision velocity selector which would directly lead to more complete angular separation of the two isotopes [19].

Velocity selection techniques can also be implemented after the atoms collide with the surface. For a given θ_f at which there is angular overlap between the ^{20}Ne and ^{22}Ne non-zeroth order diffraction peaks, the two isotopes will necessarily have different velocities, as required by equation (1). This is demonstrated in Figure 5, which shows time-of-flight spectra for both isotopes at the midway point between their (11) diffraction peak maxima. The pronounced difference in arrival time between the two isotopes opens up the possibility for complete isotope separation mediated by velocity selection techniques.

The practical throughput of diffractive isotope separation can be maximized by thoughtful consideration of the incident parameters and the choice of diffracting surface. As established by equation (1), the total number of angles at which atoms will scatter from a surface depends upon the incident wavevector of the atomic beam (k_i) and the spacing between diffraction peaks (ΔK), which is in turn dependent on the real-space distance between atoms at the surface. The incident flux of an atomic beam can be concentrated into a smaller number of accessible diffraction channels by lowering the incident wavevector/beam velocity (e.g. by nozzle cooling or seeding in a heavier gas such as xenon) or increasing the angular spread between diffraction peaks by choosing a surface with a smaller lattice parameter, such as graphite (lattice constant = 2.46 Å). We have also observed in other studies the coupling of neon with diffractive bound state resonances for this system. The resulting change in diffraction probabilities due to this phenomenon may hold additional promise for further enhancements in isotope separation.

The choice of surface can also affect the relative flux scattered into various diffraction channels. Higher ratios of scattered intensity between non-zeroth order diffraction and specular peaks have been demonstrated to be correlated with increased surface corrugation [10,20–22]. Additionally, the amount of flux that is scattered diffusely from a surface is strongly affected by the surface stiffness, which is quantified by the surface Debye temperature [14,23]. When gases diffract from surfaces with high Debye temperatures, less of the incident flux is scattered into diffuse elastic channels due to the Debye-Waller effect than for soft surfaces, resulting in a more directed channeling of the incident beam into coherent diffraction peaks. Further improvement can be realized by minimizing the surface temperature (while remaining above the physisorption limit) and thus mitigating Debye-Waller effects arising from the thermal motion of the

substrate [24,25]. In sum, the judicious selection of a well-ordered, highly perfected surface with a relatively high Debye temperature, small lattice constant, and inertness to a specific isotope or isotopologue, opens this diffractive isotope separation method to a larger class of atoms and molecules.

A practical implementation of this enrichment process would necessitate some collection scheme for the enriched product. In principle, the desired isotope can be collected with a strategically positioned cold surface where a single diffraction channel will strike and condense. Alternatively, a strategically placed aperture that admits one diffraction channel would also be a straightforward means to collect the reflected isotope from only one of the diffraction channels; this could be extended to an array of apertures placed to collect numerous higher-order (and out-of-plane) diffraction channels. Furthermore, this isotope separation technique is also amenable to recycling the diffracted beam through recompression and/or staging the diffraction process until a desired isotopic enrichment level is reached.

The angular and temporal separation effects of supersonic molecular beam diffraction provide a promising isotope enrichment method that does not require ionization or laser excitation of the target isotope. The necessity of a supersonic expansion for this technique is demonstrated, and as a proof of concept natural abundance neon has been shown to diffract into separate, isotopically dependent diffraction lab frame angles, yielding for the set of experimental conditions used herein an enrichment factor of 1.08 ± 0.03 for the major ^{20}Ne component and 3.50 ± 0.30 for the minor ^{22}Ne component in a single pass, with extension to multiple passes easily envisioned. The incomplete separation of isotopes exhibited in this work demonstrates the need for scrupulous consideration of the experimental setup to achieve maximum separation and throughput, with the velocity spread of the incident beam serving as the determining factor for

separation. As atomic diffraction has been observed for species with masses as high as 40 amu [26], this isotope separation technique is applicable to a wide range of co-expanded atoms and molecules. In sum, using a combination of a supersonic molecular beam and a well-ordered, corrugated surface with a small lattice spacing and high level of structural perfection, we have successfully demonstrated novel and efficacious routes to isotopic enrichment and separation in space and time based on gas-surface diffraction.

S.J.S. would like to acknowledge support from the Air Force Office of Scientific Research Grant No. FA9550-15-1-0428, and the Lewis group at the California Institute of Technology for providing methyl-terminated silicon.

[1] F. A. Lindemann and F. W. Aston, Philos. Mag. Ser. 6 **37**, 523 (1919).

[2] L. O. Love, Science **182**, 343 (1973).

[3] A. L. Yergey and A. K. Yergey, J. Am. Soc. Mass Spectrom. **8**, 943 (1997).

[4] T. Ruf, R. W. Henn, M. Asen-Palmer, E. Gmelin, M. Cardona, H.-J. Pohl, G. G. Devyatych, and P. G. Sennikov, Solid State Commun. **115**, 243 (2000).

[5] J.-Y. Li, C.-T. Huang, L. P. Rokhinson, and J. C. Sturm, Appl. Phys. Lett. **103**, 162105 (2013).

[6] G. N. Makarov, Phys. - Uspekhi **58**, 670 (2015).

[7] T. R. Mazur, B. Klappauf, and M. G. Raizen, Nat. Phys. **10**, 601 (2014).

[8] P. A. Bokhan, V. V. Buchanov, N. V. Fateev, M. M. Kalugin, M. A. Kazaryan, A. M. Prokhorov, and D. E. Zakrevskĭi, *Laser Isotope Separation in Atomic Vapor* (2006).

[9] J. B. Anderson, R. P. Andres, and J. B. Fenn, Adv. Chem. Phys. **10**, 275 (1966).

[10] G. Boato, P. Cantini, and L. Mattera, Surf. Sci. **55**, 141 (1976).

[11] B. Gans, P. A. Knipp, D. D. Koleske, and S. J. Sibener, Surf. Sci. **4**, 81 (1992).

[12] D. D. Koleske and S. J. Sibener, Rev. Sci. Instrum. **63**, 3852 (1992).

[13] N. T. Plymale, Y. G. Kim, M. P. Soriaga, B. S. Brunschwig, and N. S. Lewis, J. Phys. Chem. C **119**, 19847 (2015).

[14] J. S. Becker, R. D. Brown, E. Johansson, N. S. Lewis, and S. J. Sibener, J. Chem. Phys.

133, 104705 (2010).

[15] K. J. Nihill, Z. M. Hund, A. Muzas, C. Diaz, M. del Cueto, T. Frankcombe, N. T. Plymale, N. S. Lewis, F. Martin, and S. J. Sibener, J. Chem. Phys. **145**, 84705 (2016).

[16] H. Yu, L. J. Webb, R. S. Ries, S. D. Solares, W. A. Goddard, J. R. Heath, and N. S. Lewis, J. Phys. Chem. B **109**, 671 (2005).

[17] N. Isa, K. D. Gibson, T. Yan, W. Hase, and S. J. Sibener, J. Chem. Phys. **120**, 2417 (2004).

[18] G. Scoles, *Atomic and Molecular Beam Methods Volume I* (Oxford University Press, New York, 1988).

[19] C. Szewc, J. D. Collier, and H. Ulbricht, Rev. Sci. Instrum. **81**, 10 (2010).

[20] A. Politano, B. Borca, M. Minniti, J. J. Hinarejos, A. L. Vázquez de Parga, D. Farías, and R. Miranda, Phys. Rev. B **84**, 35450 (2011).

[21] K.-H. Rieder and W. Stocker, Phys. Rev. Lett. **52**, 352 (1984).

[22] M. W. Cole and D. R. Frankl, Surf. Sci. **70**, 585 (1978).

[23] E. K. Schweizer and C. T. Rettner, Phys. Rev. Lett. **62**, 3085 (1989).

[24] F. Althoff, T. Andersson, and S. Andersson, Phys. Rev. Lett. **79**, 4429 (1997).

[25] A. C. Levi, C. Huang, W. Allison, and D. A. Maclaren, J. Phys. Condens. Matter **21**, 225009 (2009).

[26] M. Minniti, C. Diaz, J. L. Fernandez Cunado, A. Politano, D. Maccariello, F. Martin, D. Farias, and R. Miranda, J. Phys. Condens. Matter **24**, (2012).

Figure Captions

Figure 1 – (a) Illustration of a monoenergetic beam of ^{20}Ne and ^{22}Ne diffracting from CH_3-Si(111) into spatially well-separated final scattering angles; (b) schematic of the ultra-high vacuum surface scattering instrument employed in this experiment; key components are a high-Mach number, triply-differentially pumped molecular beam source with variable temperature nozzle, a UHV scattering chamber with a full suite of diagnostics (not shown), and a high sensitivity triply-differentially pumped detector with a high degree of collimation, that can rotate to detect a range of final scattering angles while maintaining constant incident kinematic conditions.

Figure 2 – (a) Demonstration of angular separation for supersonic molecular beam diffraction from an ideal grating for the conditions reported herein; (b) lack of angular separation for an effusive source under identical incident conditions; T_B = 55 K, θ_i = 25.2º.

Figure 3 – Nearly complete angular separation of (11) diffraction peaks for ^{20}Ne (black) and ^{22}Ne (red) diffracted from CH_3-Si(111). Further purification of the major ^{20}Ne component or separation and enrichment of the minor ^{22}Ne component can be realized through experimental considerations as discussed in the text.

Figure 4 – (11) diffraction peak for helium (black) and ^{20}Ne (red) scattering from CH_3-Si(111). Note that the width of these peaks is a consequence of the convolution of the instrument function, surface quality, and their incident velocity distributions. The He diffraction peak has a significantly narrower angular distribution than the Ne peak, due to the narrower velocity distribution of the He beam used ($\Delta v/v$ = 0.8%) as compared to that for the Ne beam ($\Delta v/v$ = 6.4%). Potential further improvement in angular separation, as compared to the data shown in Figure 3, can be realized by additional narrowing of the beam's incident velocity distribution. Inset: wide angular range diffraction scan for He/CH_3-Si(111) demonstrating the high quality of the substrate used in these experiments.

Figure 5 – Time-of-flight spectra for ^{20}Ne (black) and ^{22}Ne (red) at the midpoint between the maxima of the ^{20}Ne and ^{22}Ne (11) diffraction peaks as shown in Figure 3, providing a route for temporal separation of the isotopes.

Figures

Figure 1:

(a)

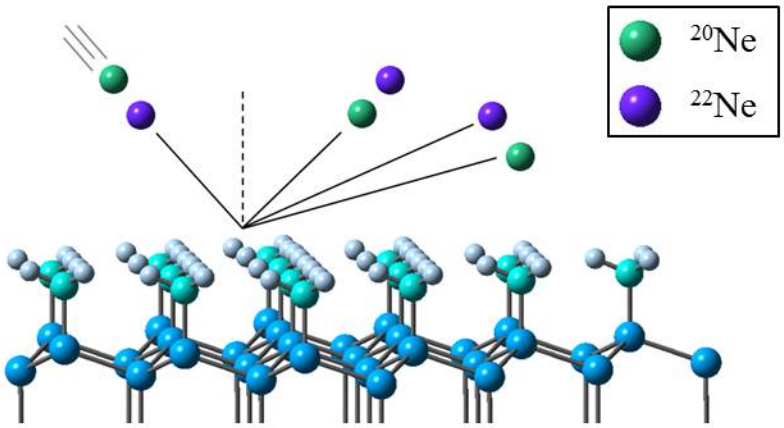

(b)

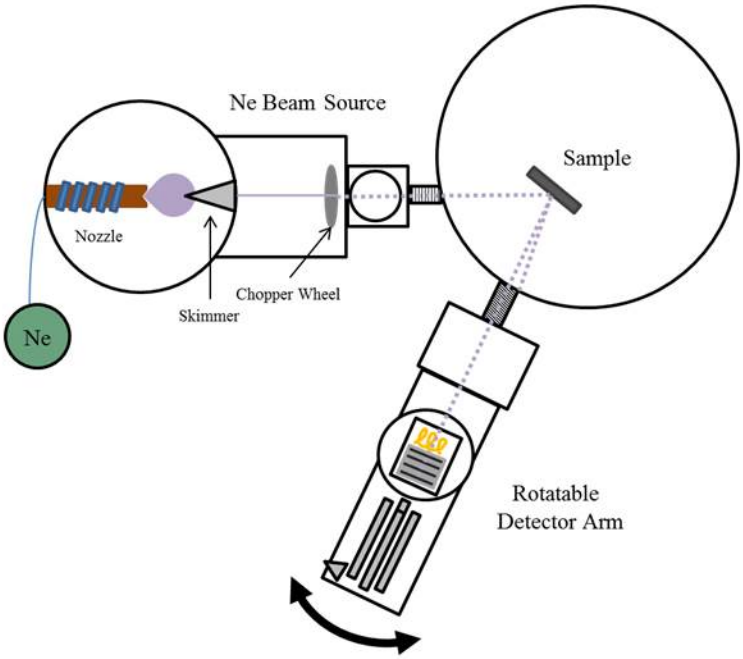

Figure 2:

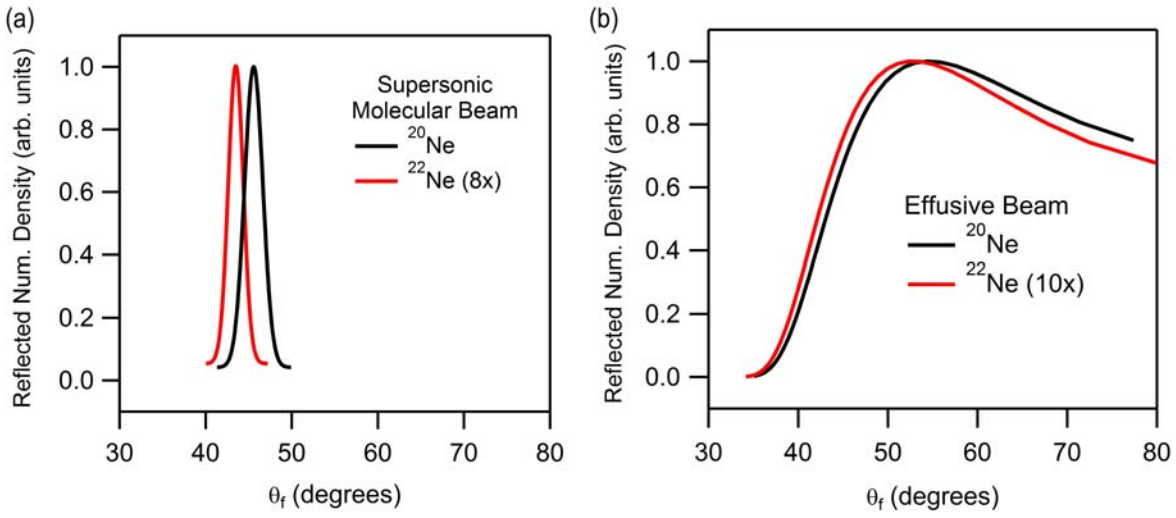
(a)
Reflected Num. Density (arb. units)
1.0
0.8
0.6
0.4
0.2
0.0
30
40
50
60
70
80
θf (degrees)
Supersonic
Molecular Beam
20Ne
22Ne (8x)
(b)
Reflected Num. Density (arb. units)
1.0
0.8
0.6
0.4
0.2
0.0
30
40
50
60
70
80
θf (degrees)
Effusive Beam
20Ne
22Ne (10x)

Figure 3:

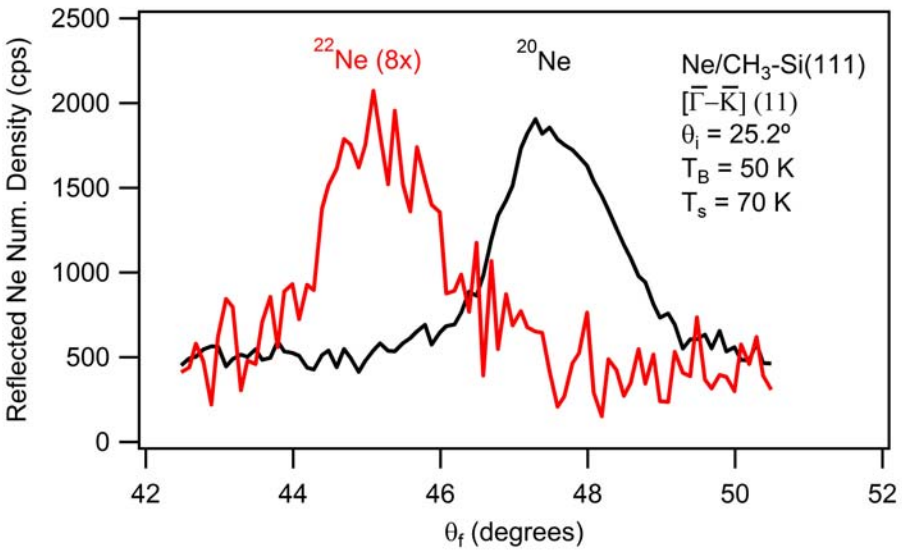
2500
2000
1500
1000
500
0
Reflected Ne Num. Density (cps)
42
44
46
48
50
52
θf (degrees)
22Ne (8x)
20Ne
Ne/CH3-Si(111)
[Γ̄–K̄] (11)
θi = 25.2°
TB = 50 K
Ts = 70 K

Figure 4:

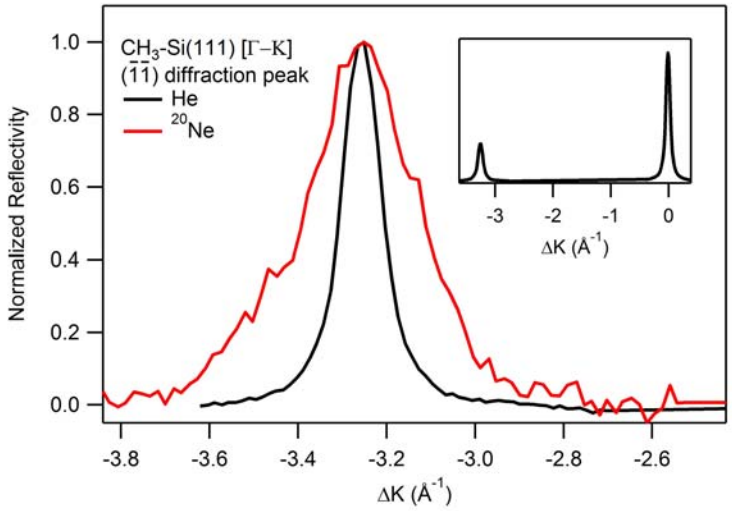
CH3-Si(111) [Γ−K]
(1̄1̄) diffraction peak
He
20Ne
Normalized Reflectivity
1.0
0.8
0.6
0.4
0.2
0.0
-3.8
-3.6
-3.4
-3.2
-3.0
-2.8
-2.6
ΔK (Å-1)
-3
-2
-1
0
ΔK (Å-1)

Figure 5:

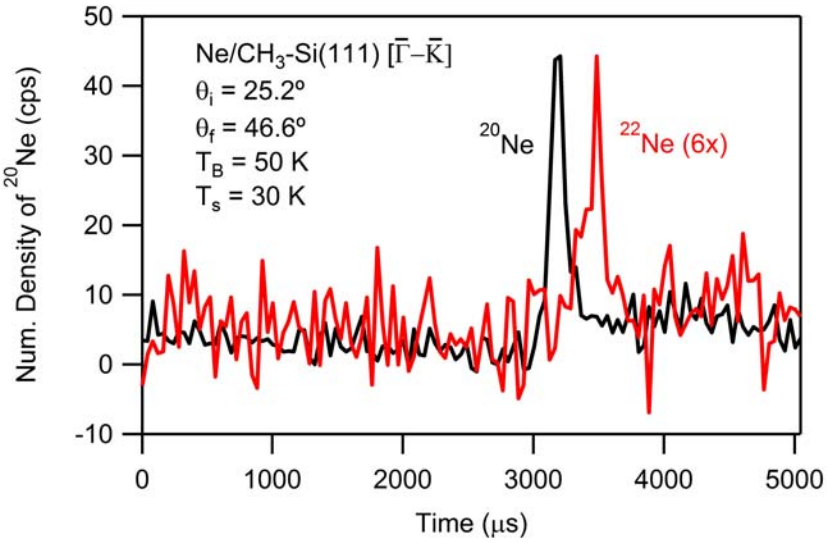
Ne/CH3-Si(111) [Γ̄–K̄]
θi = 25.2°
θf = 46.6°
TB = 50 K
Ts = 30 K
20Ne
22Ne (6x)
Num. Density of 20Ne (cps)
Time (μs)
50
40
30
20
10
0
-10
0
1000
2000
3000
4000
5000